*Sādhanā* (2021)46:29
https://doi.org/10.1007/s12046-020-01526-8

© Indian Academy of Sciences

# EBG–AMC–HIS characteristics analysis of QBTR unitcell

MARUTI TAMRAKAR* and USHA KIRAN KOMMURI

SENSE, VIT Chennai Campus, Chennai, Tamil Nadu 600127, India
e-mail: tamrakar.maruti@gmail.com

MS received 5 August 2019; revised 1 October 2020; accepted 10 October 2020

**Abstract.** In this paper the quad bend triangular resonator (QBTR) structure is used as a metamaterial unitcell for metasurface characteristics analysis. This paper presents the metasurface properties like electromagnetic band gap (dispersion diagram), reflection phase $S_{11}$ (deg) and surface impedance $Z_{11}$ ($\Omega$) of a unitcell. The unitcell analysis shows similarities in operating frequency band for these metasurface characteristics. The QBTR metasurface performance is validated using a wideband dipole antenna. The antenna gain of $> 5$ dBi is achieved with QBTR metasurface for frequency range 3.2–6.7 GHz. The QBTR metasurface is orthogonal symmetric and can be used for dual-polarized wideband frequency applications like WLAN (5.15–5.85 GHz) and NR 5G sub-6-GHz (3.3–5.0 GHz).

**Keywords.** Metasurface; EBG; AMC; HIS; reflection phase; dispersion diagram.

## 1. Introduction

The metamaterial structures (metasurface) have received considerable attention in recent years. These metasurfaces are normally periodic in nature and show characteristics of electromagnetic band gap (EBG), artificial magnetic conductor (AMC) and high-impedance surface (HIS) for a certain frequency band. The metasurfaces are considered very promising; they can be used to reduce interference, surface wave and mutual coupling and to increase directivity of antenna. The metasurface structures are also very compact in nature and can be implemented as metallic–dielectric or purely dielectric.

The traditional mushroom-like EBG structures are presented in [1] to suppress the surface wave and to increase directivity of antenna. The mushroom structure uses ground via to create metamaterial property. Multiple authors presented via-less EBG structures called as uniplanar AMC or HIS structure [2, 3]. The uniplanar structures are a square metal patch printed on PCB. These uniplanar AMC structures are used with antennas to improve antenna directivity, but they have narrow band frequency response. Instead of a square patch, a circular shaped AMC structure is presented in [4]. In uniplanar AMC structures a small conductor area is etched out such that it gives another smaller metal patch, which yields dual band response [5, 6], where the inner patch has higher band response and the outer patch has lower band response. Another method to get dual band response is by making a T-shaped slit in metal patch [7]. A notch on edges of metal patch and slot at the centre of metal patch can be implemented in AMC structures to improve their frequency bandwidth [8, 9].

The quad bend triangular resonator (QBTR) structure has been proposed by authors of an earlier work [10], where a QBTR unitcell is used to design a wideband band stop filter. In this paper the QBTR unitcell is used to analyse characteristics of AMC, HIS and EBG. The 5×5 QBTR unitcell array is implemented with a wideband dipole antenna for validation of unitcell properties. The reflection coefficient, efficiency and peak gain of the dipole antenna with the QBTR metasurface are presented in this paper. The design frequency is targeted for wireless local area network (WLAN) (5.15–5.85 GHz) and new radio (NR) 5G sub-6-GHz (bands n48, n77, n78 and n79, i.e. 3.3–5.0 GHz) applications.

## 2. Unitcell design and analysis

This section discusses the QBTR unitcell structure and its metamaterial properties.

### 2.1 *QBTR unitcell design*

The QBTR is implemented as an orthogonal symmetrical structure to achieve wide band performance. The end points of conductor traces in QBTR are bent towards the centre to increase unitcell electrical size by increasing inductance. The QBTR structure and its dimensions are shown in Figure 1, where Figure 1(a) shows the top layer conductor and Figure 1(b) shows the bottom layer conductor (ground).

*For correspondence
Published online: 04 February 2021

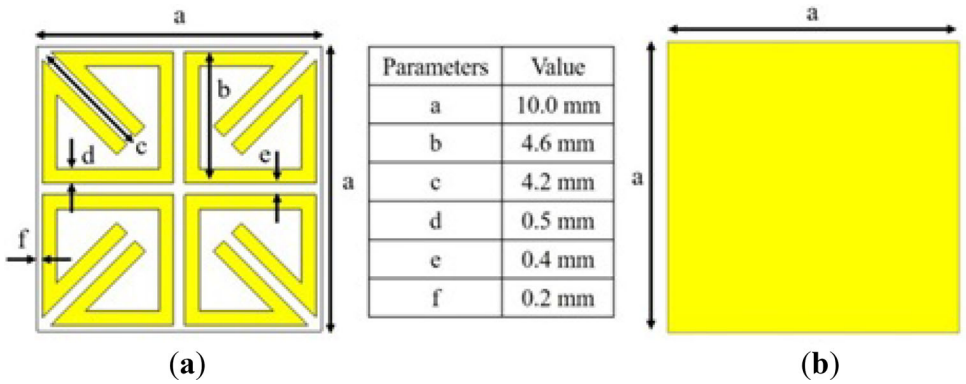


| Parameters | Value |
|---|---|
| a | 10.0 mm |
| b | 4.6 mm |
| c | 4.2 mm |
| d | 0.5 mm |
| e | 0.4 mm |
| f | 0.2 mm |

**Figure 1.** QBTR unitcell: **(a)** top layer and **(b)** bottom layer.

The design is implemented in a 10 mm × 10 mm FR4 PCB ($\varepsilon_r$ = 4.3, tan $\delta$ = 0.02) of thickness 1.524 mm. The QBTR trace width and gap between traces are maintained at 0.5 and 0.4 mm, respectively. There is capacitive coupling between the traces, which yields higher frequency bandwidth response. The orthogonal symmetrical structure supports dual orthogonal polarization.

Periodic boundaries, PEC and PMC boundaries on *x*-axis and *y*-axis, are considered with plane wave along *z*-axis in simulation. The PEC boundary aligns incident *E* field perpendicular to assigned surface, and in the same way the PMC boundary aligns incident *H* field perpendicular to assigned surface. The open port is assigned as a plane wave source, and propagation vector (*k*) is perpendicular to QBTR structure. The CST microwave studio tool is used for unitcell analysis and simulation. The plane wave gap is de-embedded till QBTR surface for *S*-parameter simulation.

The simulated unitcell *S*-parameter is shown in Figure 2(a). The reflection coefficient $S_{11}$(mag) is very high for a wide frequency band, except three frequency points of 3.7, 7.9 and 11.8 GHz. For these three frequency points the reflection coefficient $S_{11}$(mag) is close to 0.6 .The transmission coefficient $S_{21}$(mag) is zero for all frequencies, due to bottom ground in the design. The reflection coefficient and transmission coefficient show that the QBTR design is lossy ($\varepsilon_r$ = high) for the three frequency ranges 3.65–3.78 GHz, 7.45–8.48 GHz and 11 GHz–beyond. The QBTR design has the metamaterial characteristics of reflection and absorption/suppression of electromagnetic (EM) wave for certain frequency bands. These characteristics can be analysed and presented in the three ways (1) EBG: dispersion diagram, (2) AMC: reflection phase and (3) HIS: $Z_{11}$ (Ω).

The CST microwave studio tool is used for simulation, where incidence plane wave is normal to unitcell surface for AMC and HIS analysis, and time domain solver result shows the reflection phase and input impedance of the surface. For EBG the Eigen-mode solver is used, whose result shows a phenomenon of wave propagation (dispersion diagram) along the surface. In the unitcell simulation, the gap between the unitcell surface and plane wave is maintained at 7 mm, the same as dipole antenna to metasurface gap for validation (7 mm $\approx \lambda/8$ at 4.3 GHz, including substrate thickness).

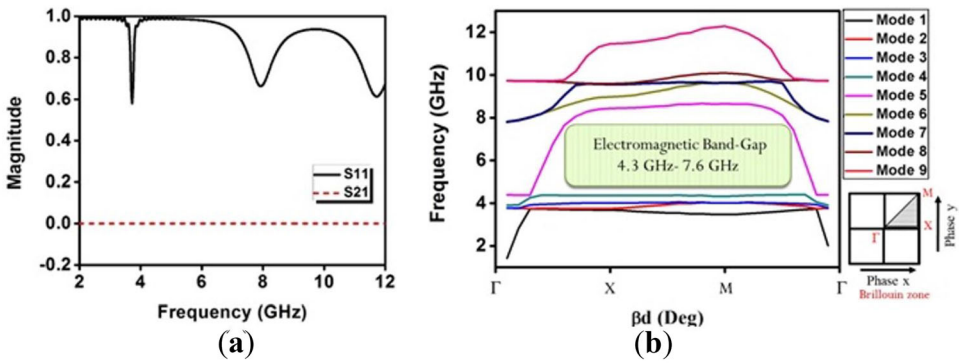


**Figure 2.** Simulated **(a)** *S*-parameter and **(b)** dispersion diagram.

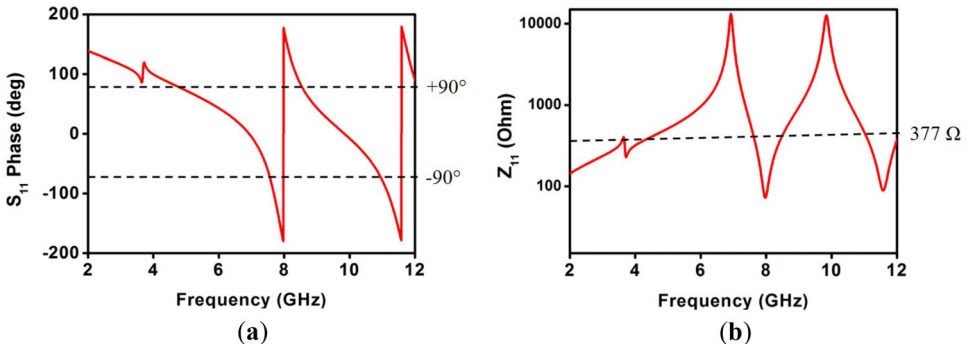


**Figure 3.** Simulated **(a)** $S_{11}$ phase (deg) and **(b)** $Z_{11}$ (Ω).

## 2.2 *EBG: dispersion diagram*

The EBG does not allow surface waves and currents to propagate for a specific frequency range. Interior to the EBG, EM waves within one or more frequency band gaps are prevented from propagating parallel to the EBG surface. The Eigen-mode solver with unitcell boundary is used in CST Simulation tool to plot dispersion diagram (in this electric field direction is normal to unitcell surface).

The dispersion diagram is composed of three parts, and each part has a unique phase shift. In the first part, *x*-axis boundary phase shift is from 0° to 180°; the *y*-axis boundary phase shift is fixed at 0°, indicted as $\Gamma - X$ part in Figure 2(b). The second part is $X - M$ part; in this, *x*-axis boundary phase shift is fixed at 180° and the *y*-axis boundary phase is shifted from 0° to 180°. The third part is $M - \Gamma$ part; in this, both *x*-axis and *y*-axis boundaries phase shift will be shifted from 0° to 180° at the same time. Figure 2(b) shows the surface characteristic frequency as a straight line superimposed over the dispersion diagram. It can be observed that the EBG frequency band is 4.3–7.6 GHz (55.46%).

## 2.3 *AMC: reflection phase*

Generally, EM plane waves are normally incident on the metasurface. For a specific frequency range the plane waves have in-phase reflection, where the tangential electric field will be reflected with phase change of 0° and the tangential magnetic field magnitude approaches zero with phase change of 180°. In practice, the useful bandwidth of metasurface is defined by the reflection phase range from +90° to −90°. The simulated reflection phase of QBTR unitcell is shown in Figure 3(a) and the result shows in-phase reflection properties for frequency ranges 4.3–7.6 GHz (55.46%) and 8.4–11.1 GHz (27.7%).

## 2.4 *HIS: $Z_{11}$ (Ω)*

The metasurface has PMC property for a particular band of frequencies, where the parallel magnetic field tends to zero, and it has a large parallel electric field on the metasurface. As a result, the metasurface provides high-impedance property to the surface for a specific frequency band and it has in-phase reflection. The bandwidth of HIS is calculated based on surface impedance, i.e. above 377 Ω (air intrinsic impedance). The surface impedance ($Z_{11}$) graph is presented in Figure 3(b) for the QBTR unitcell. The HIS frequency bandwidth follows the same AMC frequency ranges 4.3–7.6 GHz (55.46%) and 8.4–11.1 GHz (27.7%).

The unitcell analysis summary is given in Table 1. The unitcell simulation results show that the QBTR operating frequency response is the same for frequency range 4.3–7.6 GHz of all afore-mentioned three properties dispersion diagram, reflection phase and input impedance. From this analysis it is understood that the QBTR metasurface shows the characteristics of EBG, AMC and HIS for the frequency range 4.3–7.6 GHz and this metasurface can be used to reduce interference, surface wave and mutual coupling, and to increase directivity of antenna. In the next section the QBTR unitcell performance is validated with a wideband dipole antenna, and the dipole antenna is placed over the QBTR metasurface.

**Table 1.** Metasurface unitcell properties compared.

| Properties | Condition | Frequency |
|---|---|---|
| Dispersion diagram | Band gap | 4.3–7.6 GHz |
| Reflection phase | $+90° > S_{11} > -90°$ | 4.3–7.6 GHz |
| Surface impedance | $Z_{11} > 377\,\Omega$ | 4.3–7.6 GHz |

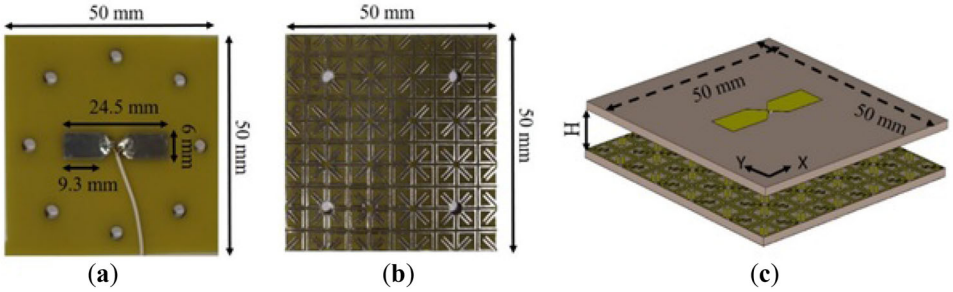


**Figure 4.** Fabricated prototype: **(a)** dipole antenna, **(b)** QBTR metasurface and **(c)** dipole assembly with QBTR metasurface.

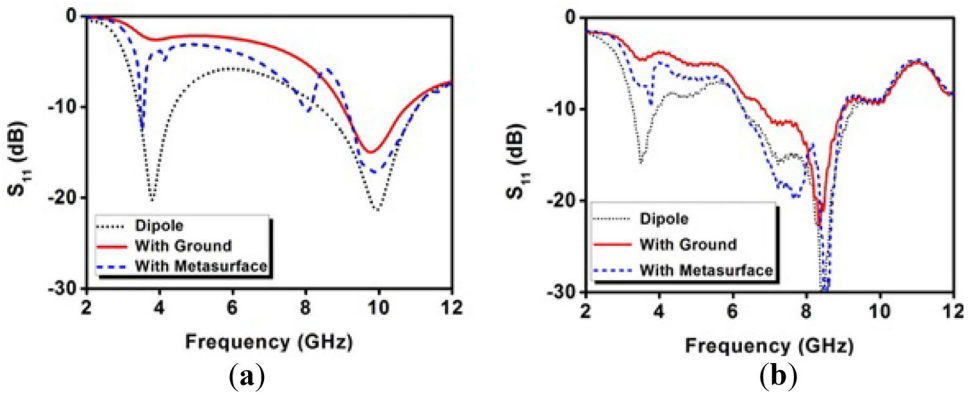


**Figure 5.** Reflection coefficient of dipole antenna with QBTR metasurface: **(a)** simulated and **(b)** measured.

## 3. Dipole antenna with QBTR metasurface

A wideband dipole is designed to analyse the impact of QBTR metasurface. The half-wavelength dipole dimension is 24.5 mm × 6 mm. The dipole antenna is implemented in FR4 substrate ($\varepsilon_r = 4.3$, tan $\delta = 0.02$, $H = 1.524$ mm) of size 50 mm × 50 mm. The resonance frequency depends on dipole length (half-wavelength, $\lambda/2$) and frequency bandwidth improves with dipole width. The dipole antenna design parameters are optimized for frequency range 3.1 GHz and higher, and –6 dB reflection coefficient $S_{11}$ (dB). The dipole antenna fabricated prototype and its dimensions are given in Figure 4(a). A 50-Ω RF coaxial cable is used to feed the dipole. The fabricated prototype of QBTR metasurface is presented (top view) in Figure 4(b).

To validate the metasurface properties of proposed unitcell the dipole antenna is placed over a 5×5 unitcell array, at gap of $H = 7$ mm ($\approx \lambda/8$ at 4.3 GHz, including substrate thickness) as shown in Figure 4(c). The 5×5 QBTR array PCB dimension is 50 mm × 50 mm. As presented in the previous section, the QBTR metasurface shows properties of in-phase reflection, HIS and EBG for the common frequency range 4.3–7.6 GHz. Hence, this frequency band is considered as the operating frequency range in subsequent sections.

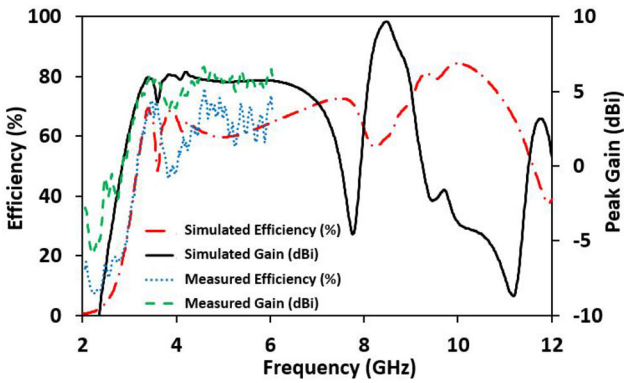


**Figure 6.** Efficiency (%) and peak gain (dBi) of dipole antenna with QBTR metasurface.

The antenna simulated $S_{11}$ (dB) is shown in Figure 5(a) and the measured graph is given in Figure 5(b). The standalone dipole antenna has $-6$ dB $S_{11}$ (dB) for frequency 3.1–12 GHz. The result shows that the dipole antenna shows wide impedance bandwidth for good $S_{11}$ ($< -6$ dB) over a wide frequency range 3.2–12 GHz and it closely matches with standalone dipole result. The dipole antenna with QBTR metasurface has better response as compared with antenna with ground.

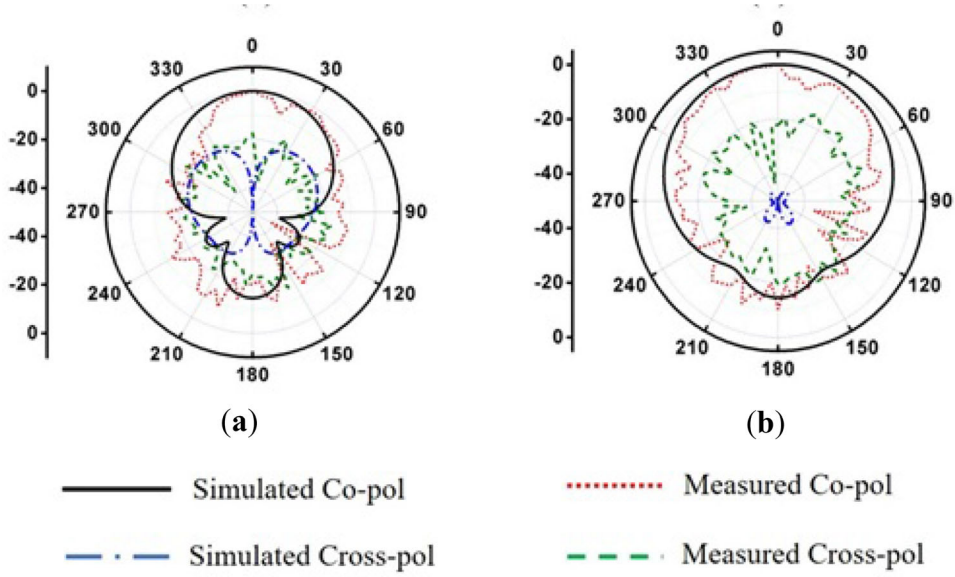


**Figure 7.** Radiation pattern of dipole antenna with QBTR metasurface at 6 GHz: **(a)** $Phi = 0^\circ$ and **(b)** $Phi = 90^\circ$.

The simulated and measured efficiency and peak gain of dipole antenna with QBTR metasurface are shown in Figure 6. The measurement data is presented till 6 GHz due to anechoic chamber higher frequency limitation. The standalone dipole antenna efficiency minimum is 70% and peak gain is 2 dBi for frequency range 3.1–12 GHz. With QBTR metasurface, the dipole antenna maintained efficiency is $> 50\%$ and gain at broadside direction ($theta = 0^\circ$) is increased to $> 5$ dBi for frequency 3.2–6.7 GHz (70.7%). The simulated antenna gain at broadside ($theta = 0^\circ$) is 9.7 dBi at 8.5 GHz. There is a small drop in antenna gain for frequency range 3.65–3.78 GHz, due to lossy behaviour of QBTR unitcell in the same frequency range. The unitcell operating frequency range (4.3–7.6 GHz) and dipole antenna gain frequency range (3.65–3.78 GHz) differ due to the antenna–metasurface assembly. The antenna is placed over QBTR metasurface at $\lambda/8$ gap, which creates a delay in EM waves resulting in effective antenna operation at lower frequency towards AMC inductive region.

The dipole antenna with QBTR metasurface has directional radiation pattern, as shown in Figure 7(a) at $Phi = 0^\circ$ cut ($xz$-plane) and Figure 7(b) at $Phi = 90^\circ$ cut ($yz$-plane). The radiation pattern is presented for frequency 6 GHz. The antenna peak gain is 6 dBi, and half-power beam-width is $57^\circ$ and $111^\circ$ in $xz$-plane and $yz$-plane, respectively. The simulated and measured cross-polarization is $-15$ dB.

## 4. Conclusion

This paper presents a unitcell analysis of QBTR metasurface for properties of EBG (dispersion diagram), AMC (reflection phase) and HIS (surface impedance). The metasurface properties like dispersion diagram, reflection phase and surface impedance have the same operating frequency range 4.3–7.6 GHz, if source to metasurface height is $\lambda/8$. The QBTR metasurface gives frequency bandwidth response of 55.46%. The QBTR metasurface is validated with the dipole antenna and antenna gain of 5 dBi is achieved for frequency bandwidth of 70.7%. The QBTR unit cell is suitable for wideband dual-polarized antenna for gain enhancement and it covers frequency bands of WLAN and NR 5G sub-6-GHz.

## References

[1] Chen D, Yang W and Che W 2018 High-Gain Patch Antenna Based on Cylindrically Projected EBG Planes. *IEEE Antennas and Wireless Propagation Letters* 17(12): 2374–2378

[2] Cai Y, Li K, Yin Y and Ren X 2015 Dual-Band Circularly Polarized Antenna Combining Slot and Microstrip Modes for GPS With HIS Ground Plane. *IEEE Antennas and Wireless Propagation Letters* 14: 1129–1132

[3] Zhu K, Su M, Yu C and Liu Y 2018 Compact High-Isolation Dual-Polarized Antenna with AMC Reflector. *Progress in Electromagnetics Research M* 73: 1–8

[4] Zhai H, Xi L, Zang Y and Li L 2018 A Low-Profile Dual-Polarized High-Isolation MIMO Antenna Arrays for Wideband Base-Station Applications. *IEEE Transactions on Antennas and Propagation* 66(1): 191–202

[5] Lin J, Qian Z, Cao W, Shi S, Wang Q and Zhong W 2017 A Low-Profile Dual-Band Dual-Mode and Dual-Polarized Antenna Based on AMC. *IEEE Antennas and Wireless Propagation Letters* 16: 2473–2476

[6] Zhai H, Zhang K, Yang S and Feng D 2017 A Low-Profile Dual-Band Dual-Polarized Antenna with an AMC Surface for WLAN Applications. *IEEE Antennas and Wireless Propagation Letters* 16: 2692–2695

[7] Ta S X and Park I 2014 Dual-Band Low-Profile Crossed Asymmetric Dipole Antenna on Dual-Band AMC Surface. *IEEE Antennas and Wireless Propagation Letters* 13: 587–590

[8] Song X Y, Yang C, Zhang T, Yan Z H and Lian R 2016 Broadband and Gain Enhanced Bowtie Antenna with AMC Ground. *Progress in Electromagnetics Research Letters* 61: 25–30

[9] Li M, Li, Q L, Wang, B, Zhou C F and Cheung S W 2018 A Low-Profile Dual-Polarized Dipole Antenna Using Wideband AMC Reflector. *IEEE Transactions on Antennas and Propagation* 66(5): 2610–2615

[10] Tamrakar M and Kiran Kommuri U 2019 Design of Compact Bend Triangular Resonator for Wide Band Application. *Progress in Electromagnetics Research Letters* 82: 1–8